Novel Peptide Inhibitors of Human Secretory Phospholipase A2 with Antiinflammatory Activity: Solution Structure and Molecular Modeling

Maung Maung Thwin,[†] Seetharama D. Satyanarayanajois,[‡] Latha M. Nagarajarao,[†] Kazuki Sato,[§] Pachiappan Arjunan,[†] Satish L. Ramapatna,[||] Prem V Kumar,[⊥] and Ponnampalam Gopalakrishnakone[†,*]

Department of Anatomy, Yong Loo Lin School of Medicine, 4 Medical Drive, National University of Singapore, Singapore 117597, Department of Basic Pharmaceutical Sciences, College of Pharmacy, University of Louisiana at Monroe, 700 University Avenue, Monroe, Louisiana 71209, Department of Chemistry, Fukuoka Women's University, Fukuoka 813-8529, Japan, Kaplan Medical, New Jersey Medical Institute, 1 Gateway Center, Newark, New Jersey 07102, and Department of Orthopaedic Surgery, Yong Loo Lin School of Medicine, 4 Medical Drive, National University of Singapore, Singapore 117597

Received April 2, 2007

Secretory phospholipase A2 (sPLA2) and matrix metallopreoteinases (MMPs) are key enzymes involved in rheumatoid arthritis (RA), and their modulation thus represents a potential therapeutic option. On the basis of *Escherichia coli* radioassay, synthetic peptides were designed and screened for sPLA2 inhibition. The linear peptide, **10f** (PIP-18), inhibited the recombinant human synovial sPLA2 activity with an IC_{50} of 1.19 μM. Not only did the peptide interfere with the function of sPLA2, but it also appeared to inhibit mRNA expression of sPLA2 and various MMPs in IL-1β-stimulated RA synovial fibroblast (RASF) cultures and thereby the production of the corresponding proteins (>80% inhibition). Nuclear magnetic resonance (NMR), modeling, and docking studies indicate that in solution the peptide exhibits a β-turn at residues Trp-Asp-Gly-Val and possibly binds to the hydrophobic channel of sPLA2. The results strongly suggest that the modulatory action of peptide **10f** may play a major role in counteracting the development of RA.

Introduction

Phospholipase A_2 (PLA2) is a key enzyme in the production of diverse mediators of inflammatory conditions and is implicated in the pathophysiology of many diseases.[1] It is an attractive target in inflammatory arthritis since it releases arachidonic acid (AA) from cell membranes, enhances cytokine induction of prostaglandin (PG) production, and is associated with enhanced release of tumor necrosis factor alpha (TNFα) and interleukin 6 (IL-6).[2] Synovial fluid from patients with rheumatoid arthritis (RA) contains high sPLA2[a] activity.[3] It has been reported that serum sPLA2 correlates with a number of disease activity markers in RA, including swollen joints, elevated platelet counts, and erythrocyte sedimentation rate.[4,5] The central role of sPLA2 in inflammatory arthritis and cancer thus makes the enzyme a potential target for drug development.

Besides the involvement of $sPLA_2$ in RA, matrix metalloproteinases (MMPs), the zinc- and calcium-dependent family of proteins produced by synovial fibroblasts, chondrocytes, and infiltrating leukocytes, have been implicated in the collagen breakdown that contributes to joint destruction in RA.[6] Several different MMPs are present in the joints of RA patients.[7] An imbalance between the active MMPs and their natural endogenous inhibitors known as 'tissue inhibitors of metalloproteinases (TIMPs)' leads to the accelerated destruction of connective tissue, which is associated with the pathology of diseases such as arthritis and cancer.[8]

A recent study demonstrates that sPLA2 enhanced the proteolytic cleavage of proMMP-2 to produce the active form of MMP-2.[9] Some PLA2 inhibitors like the chemically modified tetracyclines[10] have been reported to inhibit expression and enzymatic activity of MMPs.[11,12] A peptide that has the capacity to modulate MMPs in addition to its inhibitory potency against sPLA2 can be useful in early stages of disease onset to achieve improved clinical advantage over the use of sPLA2 or MMP inhibitors alone in the treatment of RA. In our earlier report we have shown that a 17-residue synthetic peptide P-NT.II[13] designed from the snake serum protein termed phospholipase A2 inhibitor protein (PIP)[14] could inhibit sPLA2 activity and suppress inflammation as well as cartilage and bone erosion components of arthritis in a clinically relevant transgenic mouse model.[15] The present study was undertaken to search for more potent novel peptide inhibitors using an *in vitro* screening approach of short peptide analogues of PN-T.II, coded here as **1** (PIP-17). To understand the structure−function relationship of peptides, we also carried out detailed NMR and molecular modeling studies of the designed peptides. Our results indicate that the designed peptides are useful for modulation of the arthritic inflammation.

Results

Screening of Peptide Analogues. The 17-mer linear peptide **1** that was derived from residues 56−72 of PIP[14] was used in this study as a control peptide to determine which features of its sequence are important for human sPLA2-IIA inhibition. Earlier, we reported that peptide **1** (previously termed PN-T.II) dose-dependently inhibited the activity of human sPLA2-IIA

* Author to whom correspondence should be addressed. E-mail: antgopal@nus.edu.sg.
[†] Department of Anatomy, Yong Loo Lin School of Medicine.
[‡] University of Louisiana at Monroe.
[§] Fukuoka Women's University.
[||] Kaplan Medical, New Jersey Medical Institute.
[⊥] Department of Orthopaedic Surgery, Yong Loo Lin School of Medicine.

[a] Abbreviations: AP-1, activator protein-1; CD, circular dichroism; C/EBP, CCAAT/enhancer binding protein; DMSO-d_6, deuterated dimethyl sulfoxide; DMEM, Dulbecco's Modified Eagle's Medium; ERK, extracellular-regulated kinase; FBS, fetal bovine serum; FLSC, fibroblast-like synovial cells; IC_{50}, half maximal inhibitory concentration; JNK, c-jun N-terminal kinase; LGA, Lamarckian Genetic algorithm; MAPK, mitogen-activated protein kinase; MMPs, matrix metalloproteinases; ms, millisecond; NF-κB, nuclear factor-kappa B; OA, osteoarthritis; PPAR, peroxisome proliferator-activated receptor; RASF, rheumatoid arthritis synovial fibroblast; RA, rheumatoid arthritis; rmsd, root mean square deviation; sPLA2, secretory phospholipase A2; Tg197, transgenic mice 197. Single-letter and three-letter abbreviations are used for amino acids.

10.1021/jm070385x CCC: $37.00
Published on Web 11/01/2007

Table 1. Polypeptide Analogues of sPLA2-Inhibitory Peptide **1**[a]

polypeptide variants	sequence	mol wt	% inhibition (mean ± SD)	IC_{50} [μM] (mean ± SD)
1 (PIP-17)	^{56}LGRVDIHVWDGVYIRGR^{72}	2011	55.61 ± 2.29	5.30 ± 1.12
2 (scrambled **1**)	YRRVDIGLRVWHDLGVG	2011	Ns	ND
3	^{56}LGRVDIHVWDGVYIRG^{71}	1855	52.41 ± 3.45	5.60 ± 1.32
4	^{56}LGRVDIHVWDGVYIR^{70}	1798	50.95 ± 2.28	5.75 ± 1.46
5	^{56}LGRVDIHVWDGVYI^{69}	1642	49.70 ± 3.61	5.80 ± 1.61
6	^{56}LGRVDIHVWDGVY^{68}	1528	48.66 ± 4.12	5.95 ± 1.54
7	^{56}LGRVDIHVWDGV^{67}	1365	34.21 ± 5.65	insoluble
8	^{57}GRVDIHVWDGV^{67}	1252	14.22 ± 2.87	insoluble
9	^{58}RVDIHVWDGV^{67}	1195	59.47 ± 3.29	3.67 ± 1.25
10 (PIP-9)	^{59}VDIHVWDGV^{67}	1039	56.37 ± 1.21	3.80 ± 1.06
11	^{60}DIHVWDGV^{67}	940	45.85 ± 2.43	5.75 ± 0.96
12	^{61}IHVWDGV^{67}	825	35.40 ± 2.22	6.21 ± 1.02
13	^{61}IHVWDG^{66}	726	ns	ND
14	^{62}HVWDG^{66}	613	ns	ND

[a] % inhibition determined against purified human synovial $sPLA_2$ (Cayman Chemicals, Ann Arbor, MI) at a fixed peptide concentration (5 μM) using ^{3}H-labeled *E. coli* membrane assay. IC_{50} (mean ± SD) determined from sigmoid inhibition curves (Gradpad Prism). ND = not done; ns = not significant. Statistical analyses done by one-way ANOVA using Dunnet's multiple comparison test. **1** versus **3**, **4**, **5**, **6**; **9** versus **10** = not significantly different ($P > 0.05$); **10** versus **11**, **12** = significantly different ($P < 0.05$). Superscript numbers on both sides of each peptide sequence indicate amino acid spans of the native PIP protein. For NMR and docking studies the numbering scheme was used with N-terminal residue starting from residue number 1.

Table 2. Peptide Variants of sPLA2-Inhibitory Peptide **10**[a]

peptide variants	sequence	Mol. wt.	% inhibition (mean ± SD)	IC_{50} [μM] (mean ± SD)
10	^{59}VDIHVWDGV^{67}	1039	56.37 ± 1.21	3.80 ± 1.06
10a	^{59}VDIHVWAGV^{67}	995	48.52 ± 1.34	5.45 ± 1.98
10b	^{59}VDIHVWEGV^{67}	1053	57.62 ± 2.22	4.95 ± 2.22
10c	^{59}VDIHVWSGV^{67}	1011	52.55 ± 0.58	5.25 ± 3.21
10d	^{59}VDIHVWDbGV^{67}	1039	49.71 ± 1.01	5.55 ± 1.21
10e (PIP-9cy)	C-VDIHVWDGV-C	1243	ns	ns
10f (PIP-18)	VDIHVWDGV-VDIHVWDGV	2060	74.55 ± 4.21	1.19 ± 0.55

[a] % inhibition determined against purified human synovial $sPLA_2$ (Cayman Chemicals, Ann Arbor, MI) at a fixed peptide concentration (5 μM) using ^{3}H-labeled *E. coli* membrane assay. IC_{50} (mean ± SD) was determined from sigmoid inhibition curves (Gradpad Prism). ns = not significant. Statistical analyses done by one-way ANOVA using Dunnet's multiple comparison test. **10** versus **10a**, **10c**, **10d**, **10f** = significantly different ($P < 0.05$); **10** versus **10b** = not significantly different ($P > 0.05$).

(IC_{50}, 6.3 ± 0.80 μM) through its specific interaction with the sPLA2 enzyme, while it was less effective in inhibiting cytosolic (c) PLA2 (IC_{50}, 23.91 ± 2.39 μM). The negative control peptide **2** with a scrambled sequence of **1** was noninhibitory to human sPLA2 and it failed to block its binding to immobilized sPLA2s.[13] Here, we synthesized peptide analogues containing single amino acid deletions and evaluated their inhibitory activity of sPLA2 in a high throughput enzyme activity screening assay relative to the control peptide **1**. The inhibition properties of all the peptides screened are shown in Table 1. The present screening procedure involving reduction of the length of peptide **1** from both N- and C-termini did not result in a significant decrease of inhibition in the *Escherichia coli* assay (**1** *versus* **3**−**6**, $P > 0.05$). The insolubility of the two analogues in the enzyme reaction buffer (**7** was only sparingly soluble while **8** was totally insoluble) may account for their loss of activity in the inhibition assays. The peptide **9** representing the sequence (^{58}RVDIHVWDGV^{67}) showed the maximal inhibition, and the removal of arginine (R) at residue 58 in **10** did not significantly reduce its effective inhibition (**9** *versus* **10**, $P > 0.05$). Deletion of residues from the left or right termini of **10** resulted in further decrease in inhibition potency, thus suggesting that peptide **10** with the shortest segment (^{59}VDIHVWDGV^{67}) may most probably be the minimal structure required to represent the pharmacophore of the PIP molecule.

Peptide Variants of 10. A number of side-chain replacement analogues of **10** were then made at position 65 as shown in Table 2. Using a β-isoform of aspartic acid (**10d)** resulted in significant reduction of inhibition relative to the α-isoform, confirming that the spatial relationship to the peptide backbone is also important for sPLA2 inhibition. Replacement of aspartic acid (D) with alanine (A) or serine (S) (**10a**, **10c**) decreased the inhibition of sPLA2 substantially, whereas substitution of Asp (D) with the similarly charged glutamic acid (E) (**10b**) retained inhibition, suggesting that a negative charge is necessary at this position in the peptide. Next, we designed, synthesized, and evaluated a multimeric peptide **10f** (PIP-18), containing two copies of **10**. When the inhibitory activity of **10** and **10f** was compared, the latter more effectively inhibited human synovial sPLA2 than the former peptide. The overall results indicate that the peptide **10f** has the strongest inhibitory activity against the purified human synovial sPLA2, while the cyclic peptide **10e** was noninhibitory.

CD Spectra of Peptides. CD spectra of the peptides (**1**, **10**, and **10e**) are shown in Figure 1. The peptides **10** and **10e** exhibit a negative CD band around 198−200 nm, indicating the possibility of an open or flexible conformation of the peptide. Peptide **1** exhibits a negative CD band around 202 nm, suggesting the possibility of a β-turn conformation of the peptide.[16] Peptide **10f** exhibited a negative band around 217 nm and a positive band around 200 nm, indicating the stable β-sheet conformation of the peptide[17] (Figure 2). On the basis of the overall conformation of the peptides in solution, peptide **10f** has a stable secondary structure, while other peptides exhibit only a small percentage of β-turn structure.

NMR and Conformation of the Peptides. To understand the detailed conformation of the peptides in solution, NMR studies of the peptides were carried out using two solvent systems (50% water and 50% dimethyl sulfoxide (DMSO), and 100% DMSO) because of the poor solubility of the peptides in water. One-dimensional and two-dimensional spectra of the peptides in both solvent systems were similar, indicating that the overall conformation of the peptide was similar in the two solvent systems.

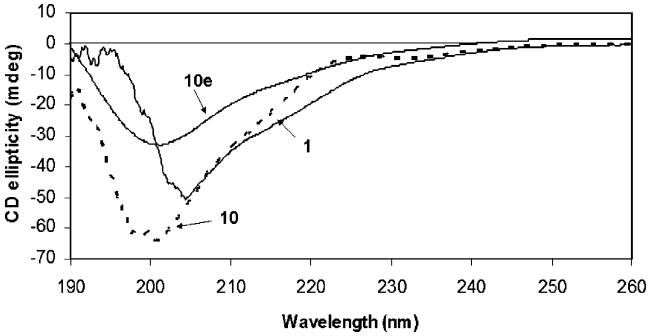

Figure 1. CD spectra of **10** (PIP-9), **1** (PIP-17), and **10e** (PIP-9Cy) peptides in water (10 μL of DMSO in 300 μL of water). Concentration of the peptide was 0.15 mM.

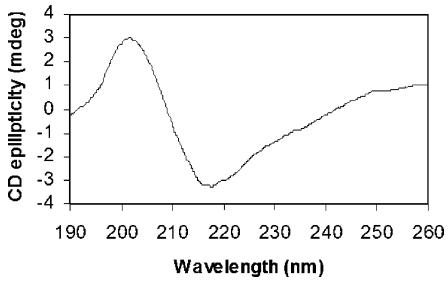

Figure 2. CD spectrum of peptide **10f** in water (10 μL of DMSO in 300 μL water). Concentration of the peptide was approximately 0.15 mM. Concentration of the peptide could not be determined accurately, as the peptide solubility was poor. The sample was filtered before collecting the CD data to avoid noise due to scattering.

Peptide 10. The 1D and 2D NMR spectra of this peptide showed well dispersed NMR resonances in the amide region (>1 ppm).[18] The coupling constant $^3J_{HN\alpha}$ of most of the amide resonances were greater than 7.5 Hz, indicating extended structure of the peptide or conformations which are rapidly interconverting. Val9 showed a large value of coupling constant of 8.5 Hz. The nuclear Overhauser effect spectroscopy (NOESY) spectrum showed NH−NH (i to i+1) connectivities for resonances from Ile3 to Val9. The temperature coefficient of chemical shift of amide resonances of His4, Val5, and Gly8 were less negative than −3 ppb/K, indicative of solvent-shielded or intramolecularly hydrogen bonded amide protons.[19] The chemical shift index data[20] of C_α protons suggest that the N-terminal part of the peptide has an extended or β-sheet type of structure, whereas the C-terminal part of the peptide (Trp6-Asp7-Gly8-Val9) has a folded helical or turn type of structure. Based on the NOESY distance constraints and coupling constant data, a model was proposed for **10** using 50 NOE constraints and 17 dihedral angle constraints in the calculations. The peptide exhibits an extended structure from Val1 to Val5 and a β-turn structure[21] from Trp6 to Val9 (Figure 3A). The root-mean-square (rms) deviation of the backbone for 20 structures was 1.41 Å, and all the structures exhibited a stable β-turn around the residues Trp6-Asp7-Gly8-Val9. The rms deviation around the β-turn residues for backbone atoms of 12 structures was 0.73 Å (Figure 3B).

Peptide 1. This peptide exhibited a well dispersed chemical shift of amide resonances (>1 ppm dispersion of chemical shift). Most of the amide resonances showed NH−NH and NH−C_αH connectivities. Coupling constants in the range of 7−8 Hz were indicative of averaged structure in solution. An NOE observed between the amide proton of Trp9 and Val12 was indicative of a folded structure. Eighty-five inter- and intraresidue NOEs were

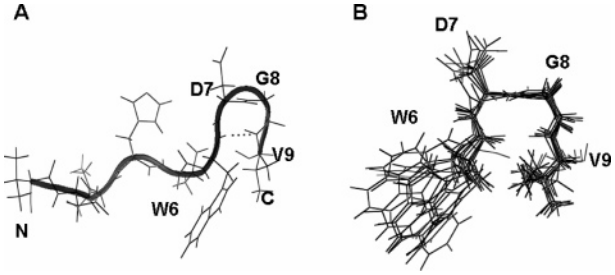

Figure 3. (A) Average structure of peptide **10** (PIP-9) obtained from NMR restrained MD simulation and energy minimization. Adjacent to each amino acid residues of the peptide **10**, numbers (1 to 9) are assigned across N- to C-terminal. Residues involved in β-turn are shown with labels. Hydrogen bonds are shown by dotted line. (B) 12 overlapped structures of β-turn region of peptide **10** showing stable nature of the turn region.

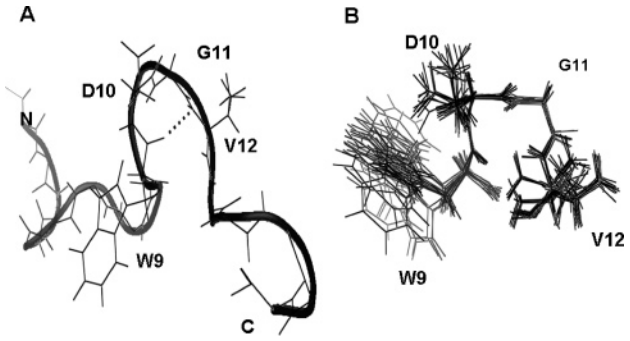

Figure 4. (A) Average structure of peptide **1** (PIP-17) obtained from NMR restrained MD simulation and energy minimization. Numbers 1 to 17 are assigned (across N- to C-terminal), adjacent to each amino acid residues of the peptide **1**. Residues involved in β-turn are shown with labels. Hydrogen bonds are shown by dotted line. (B) Twenty overlapped structures of β-turn region of peptide **1** showing stable nature of the turn region.

used in the calculation of the structure of peptide **1** along with 32 dihedral angle constraints. The peptide exhibits a β-turn structure around the residues Trp9-Asp10-G11-Val12 (Figure 4A). The rms deviation of the backbone atoms 20 structures was 2.1 Å, and for the residues in the β-turn of 20 structures was 0.30 Å, indicating the stable nature of the β-turn structure in solution (Figure 4B).

Peptide 10f. The peptide exhibited a well-dispersed NMR chemical shift of the amide resonance over a range of more than 1 ppm. However, the assignment was complicated by the repeating sequence of the peptide from Val10 to Val18. Assignment of similar type of residues was carried out by sequential connectivities in the NOESY spectra. There were few overlapping resonances in the amide region of the spectrum acquired in 500 MHz NMR spectrum at 298 K. To resolve the overlapping of resonances, NMR spectra were collected in high-resolution 800 MHz NMR instrument at three different temperatures (298, 305, and 315 K) in DMSO solvent. A total of 256 distance constraints and 34 dihedral angle constraints were used to calculate the **10f** structure. The peptide exhibited two β-turns at Trp6-Asp7-Gly8-Val9 and Trp15-Asp16-Gly17-Val18, which fold the peptide into a β-sheet type of structure (Figure 5). The β-turn structure at Trp15-Asp16-Gly17-Val18 was flexible compared to the β-turn at Trp6-Asp7-Gly8-Val9. The β-sheet structure or folded structure of the peptide was supported by an NOE between Val14 C_αH proton to His4 C_αH proton. The rms deviation of the backbone atoms of all the residues for 20 structures was 1.95 Å, indicating the

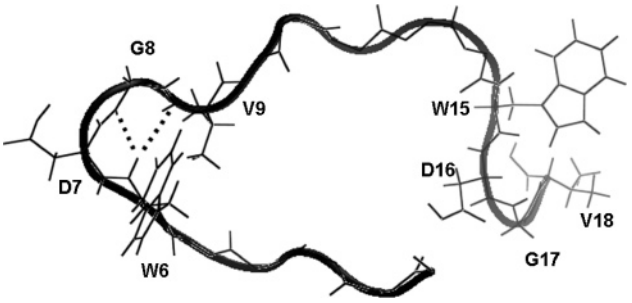

Figure 5. Average structure of peptide **10f** (PIP-18) obtained from NMR restrained MD simulation and energy minimization. Numbers 1 to 18 are assigned (across N- to C-terminal), adjacent to each amino acid residues of the peptide **10f**. Residues involved in β-turn are shown with labels. Hydrogen bonds are shown by dotted line.

overall flexible nature of the peptide structure. However, the β-turn structure of the peptide was stable in most of the structures.

Peptide 10e. The rotating frame Overhauser effect spectroscopy (NOESY) NMR spectrum of the cyclic peptide (**10e**) showed NH−C_αH connectivities for most of the residues. However, NH−NH region did not exhibit any cross-peaks, suggesting that **10e** is flexible or that different conformations of the peptide are rapidly interconverting in solution. Since the peptide is intermediate in size with a molecular weight of 1243, and may be in the zero-NOE region, an ROESY experiment was performed. However, the ROESY spectrum indicated similar results. Because of the lack of NH−NH connectivities and the small number of NOEs, the three-dimensional structure of peptide **10e** was not calculated.

Docking Studies. Docking of each peptide to sPLA2 using autodock resulted in several possible conformers. Although the C_α atom of F5 was chosen as the center of the grid in autodock calculations, the grid covered the protein crystal structure encompassing the volume of 128 Å in each direction from the center of the grid. This ensures that any possible position in that region can be considered as a binding site. The two low energy docked structures were evaluated for the possible binding site of peptide on sPLA2. The energy values, location of the peptide on sPLA2 protein, and hydrogen bonding interactions of the low energy docked structures are shown in the Table 3. The lowest docked energy structure was regarded as possible binding site of the peptide on sPLA2 protein. To avoid confusion of the nomenclature of peptide and protein residues, we have used a single-letter code for protein residues and three-letter codes for peptide residues in the running text of the manuscript.

Peptide 10−sPLA2 complex. The lowest docked energy structure of **10** had a docked energy of −8 kcal/mol. The β-turn of the peptide was located near the N-terminal part of the sPLA2 protein (Figure 6A). The Trp6 of the peptide was buried in the hydrophobic cavity of the protein formed by F5, I9, F98, Y21, and A17. There was only one hydrogen bonding interaction between the peptide and the protein. Asp7 of the peptide formed a hydrogen bonding interaction with the R7 side chain of the protein. The second lowest energy docked structure had a docked energy of −7.3 kcal/mol. In this case, the orientation of the peptide was slightly changed compared to the lowest energy structure. The β-turn of the peptide was buried in the hydrophobic pocket with Gly8 and Val9 forming a hydrophobic interaction with the peptide. To compare the binding of peptides, we analyzed the crystal structure of a complex of sPLA2 with its inhibitor indole.[22] In the crystal structure of the complex, the indole molecule is placed near the N-terminal part of the sPLA2 protein that is interacting with the hydrophobic channel-forming residues Y51, K62, L2, F5, I19, A17, Y21, F98, and V30. In the case of the peptide **10**−sPLA2 complex, the β-turn residues seem to be important in binding to the hydrophobic binding pocket and stabilizing the peptide−protein complex.

Peptide 1−sPLA2 Complex. In this case, the lowest energy docked structure had energy of −13.3 kcal/mol. However, β-turn of the peptide **1** was not involved in the interaction with hydrophobic pocket of the protein. The N-terminal part of it was near the hydrophobic pocket of sPLA2. Leu1 of the peptide was buried in the hydrophobic pocket formed by residues F5, I9, F98, Y21, and A17 (Figure 6B). There were three hydrogen bonds between the peptide and the protein contributing toward the lowest docked energy of the peptide. The second lowest energy structure has energy of −9.9 kcal/mol. In this possible binding mode, the β-turn of the peptide was near the N-terminal part of the sPLA2 protein. The Trp9 of the peptide was buried in the hydrophobic pocket of the protein.

Peptide 10f−sPLA2 Complex. For this peptide, docking studies resulted in two lowest energy structures that had nearly the same energy (−4.5 kcal/mol and −4 kcal/mol). Analysis of the results indicates that there are two possible modes of binding of peptide to sPLA2 protein. The docked structures with −4.5 kcal energy had β-turn Trp6-Asp7-Gly8-Val9 near the hydrophobic pocket of the protein. His4 and Val5 of the peptide were buried in the hydrophobic pocket of the protein formed by residues Y51, K62, L2, F5, I19, A17, Y21, F98, and V30 (Figure 6C). There was only hydrogen bonding interaction between the Asp7 of the peptide to H6 of the protein. In the second mode of binding with docked energy of −4 kcal/mol, Trp15 was near the hydrophobic pocket with Trp15 and Val18 buried in the hydrophobic pocket of the protein (Figure 6D). The Ile3, His4, and Asp11 of the peptide formed hydrogen bonding interaction with F63, S65, and K62 of the sPLA2 protein.

Peptide Suppression of sPLA2 and MMP Production in RASF. Enzyme Linked immunosorbent assay (ELISA) was used to examine the effect of **10f** and LY315920 (**15a**) (selective sPLA2 inhibitor) on the suppression of IL-1β-induced sPLA2 and MMP protein expression in human RA synovial fibroblasts (RASF). When assessed for viability to peptide treatment using sodium 3,3′-[1-[(phenylamino)carbonyl]-3,4-tetrazolium]-bis(4-methoxy-6-nitrobenzenesulfonic acid hydrate) (XTT) Cell Proliferation Kit II (Roche Applied Science, Indianapolis, IN), human RASF were nontoxic after 24 h treatment at the doses used (1, 5, and 10 μM) in our RASF cultures (data not shown). As shown in Figure 7A, dose-dependent inhibition of IL-induced sPLA2 production was observed with **10f** at the three dose levels (1, 5, and 10 μM) tested. Since sPLA2 production was significantly inhibited by the peptide at 5 μM (1 μM vs 5 μM $p < 0.5$; 5 μM vs 10 μM $p > 0.05$), a fixed final concentration of 5 μM peptide was used for all later experiments with RASF cultures. Figure 7B shows the suppressive effect of **10f** on cytokine-induced production of sPLA2 in comparison with that of a highly selective and specific sPLA2 inhibitor, **15a**. As compared to levels observed in unstimulated RASF, sPLA2 production was markedly increased to nearly 10-fold after stimulation with IL-1β. This elevated sPLA2 production was significantly suppressed with both the peptide **10f** ($p < 0.001$) and the positive control indole sPLA2 inhibitor **15a** ($p < 0.01$) at a final concentration of 5 μM. Because of very low levels of sPLA2-IIA measured in unstimulated cells, the effect of peptide on sPLA2 production observed in those cells was not significant.

Consistent with the elevated expression of sPLA2 after stimulation of RASFs with IL-1β, marked generation of MMPs (MMP-1, MMP-2, MMP-9) was also observed at 24 h (Figure

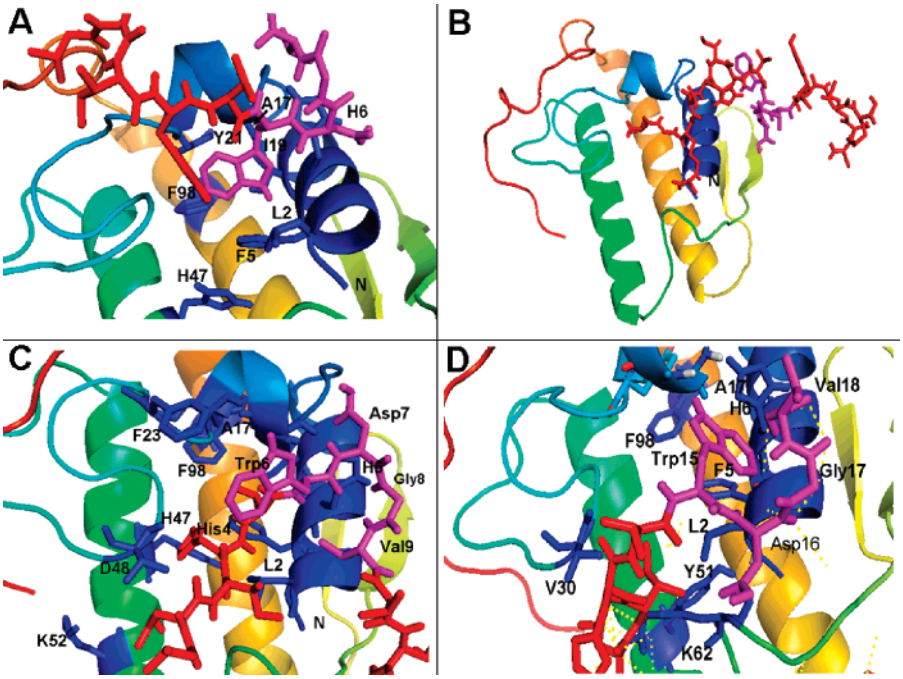

Figure 6. Proposed model for the sPLA2 protein−peptide complex from docking studies. Protein is shown in secondary structure representation. Peptide is shown as sticks. Side chain of residues that forms the hydrophobic cavity and that are important in interaction with peptide are shown. Numbers 1 to 18 are assigned (across N- to C-terminal), adjacent to each amino acid residues of the peptide **10f**. (A) Low energy docked structure of peptide **10** with sPLA2 crystal structure showing interactions. β-Turn of the peptide is shown in magenta. Note that Trp6 of the peptide interacts with the hydrophobic cavity in the protein. (B) Low energy docked structure of peptide **1** with sPLA2 crystal structure. β-Turn of the peptide is shown in magenta. Note that the N-terminal part of the peptide interacts with the hydrophobic cavity of the protein. (C) First mode of binding of peptide **10f** with sPLA2 (docked energy −4.5 kcal). β-Turn of the peptide (Trp6-Asp7-Gly8-Val9) is shown in magenta. His4 of the peptide is buried in the hydrophobic cavity. For the sake of clarity, side chains of protein are labeled with single letter amino acid code, and peptide side chains are labeled with three-letter amino acid code. (D) Second mode of binding of **10f** with sPLA2 (docked energy −4.0 kcal). The second β-turn of the peptide (Trp15-Asp16-Gly17-Val18) is shown in magenta.

Table 3. Low Energy Docked Structure of the Peptides[a]

peptide	docked energy, kcal/mol	position of the ligand (peptide) with respect to binding pocket in sPLA2 crystal structure	hydrogen bonding interaction	
			peptide	protein
10 (1)	−8.0	Trp6 buried in the hydrophobic pocket formed by F5, I9, F98,Y21 and A17	Asp7 Oδ (sc)	R7 Hη (sc)
10 (2)	−7.3	Gly8, Val9 buried in the hydrophobic pocket	Val9 COOH (bb) Asp7 Oδ (sc)	L2 CO (bb) V30 NH (bb)
1 (1)	−13.3	N-terminal region of the peptide near the hydrophobic pocket. Leu1 of the peptide buried in the pocket.	Asp10 Oδ (sc) Arg3 Hη (sc) Gly2 CO (bb)	R7 Hη (sc) K62 CO (bb) L2 NH (bb)
1 (2)	−9.9	Trp9 buried in the hydrophobic pocket.	Asp5 Oδ (sc) Gly2 NH (bb) Arg17 NH (bb)	H6 Hϵ(sc) E16 Oϵ (sc) F63 CO (bb)
10f (1)	−4.5	Trp6 near the pocket. His4 and Val5 buried in the hydrophobic pocket	Asp7 Oδ (sc)	H6 Hϵ(sc)
10f (2)	−4.0	Trp15 near the pocket.	Ile3 NH (bb) His4 Hϵ (sc) Asp11 Oδ (sc)	F63 CO (bb) Ser65 CO (bb) K62 Hζ (sc)

[a] bb, backbone, sc, side chain; peptide residues are labeled with a three-letter code, and protein residues are labeled with a one-letter code for amino acids.

8). These elevated levels of MMP-1, MMP-2 and MMP-9 were significantly suppressed by 1 h pretreatment of RASF with **10f** ($p < 0.001$, one-way analysis of variance (ANOVA) with Dunnet's multiple comparison post test) or with **15a** ($p < 0.01$), suggesting the beneficial effect of sPLA2 inhibition in suppressing sPLA2-dependent augmentation of IL-induced MMP production by these RASFs (Figure 8, A, B, C). In contrast to the suppressive effect of the peptide **10f** or **15a** on MMP generation, none of the inhibitors had any effect on TIMP-2 production by IL-stimulated RASFs (Figure 8D).

Peptide Effect on Gene Expression in RASF. In order to examine the potential suppression of sPLA2 and MMP gene expression by the peptide **10f**, we used the quantitative reverse transcription polymerase chain reaction (QRT-PCR) for assessing relative mRNA expression levels of IL-1 β-induced rabbit normal FLSC and human RASF in the presence and absence of **10f** (Figure 9). The thermalcycler-PCR for glyceraldehyde-3-phosphate dehydrogenase (GAPDH) and other genes showed a single (peak) product, indicating that no false amplification occurred (data not shown). Each gene was normalized against

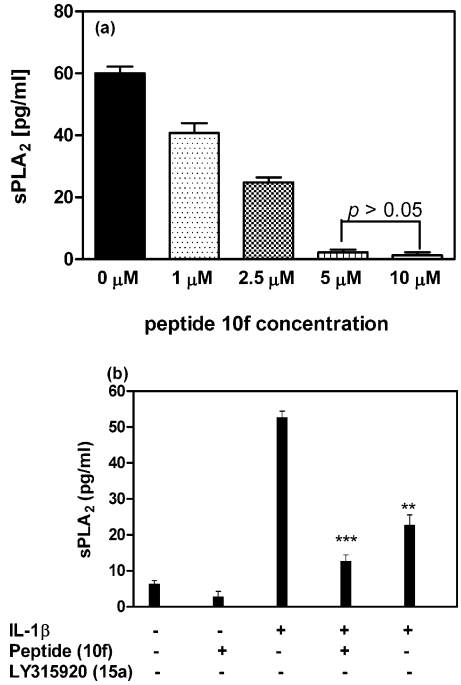

Figure 7. Inhibition of IL-1β-induced release of sPLA2 protein by peptide **10f** in human RASF. Human RASF were preincubated (1 h, 37 °C) with vehicle (final 0.1% DMSO), **10f** (5 μM), or **15a** (5 μM), and the incubation was continued for a further 24 h with or without IL-1β (10 ng/mL) as indicated. sPLA2 protein levels (pg/mL) were measured afterward in culture supernatants using sPLA2 human type IIA EIA kit (Cayman). Treatment with (IL-1β + **10f**) or (IL-1β + **15a**) was compared with IL-1β-stimulated sample (without inhibitor) to perform one-way ANOVA test with a *post hoc* test done using a Dunnet's multiple comparison test. Results with the statistical significance of $p < 0.05$ (*), $p < 0.01$ (**), $p < 0.001$ (***) are indicated. Results are the mean ± SD of triplicate determinations from a representative experiment of three RASFs. (A) Dose-dependent inhibition of IL-induced sPLA2 production by **10f** peptide, determined at four dose levels (1, 2.5, 5, and 10 μM). (***1 μM *versus* 5 μM; 5 μM *versus* 10 μM, $p > 0.05$). (B) Suppressive effect of **10f** on IL-1β-induced production of sPLA2 in comparison to that of a highly selective and specific sPLA2 inhibitor, **15a**. Elevated sPLA2 production was significantly suppressed with both the peptide **10f** *** and the positive control **15a** **.

the housekeeping gene GAPDH and was shown as relative fold increase or decrease. Greater than 1.5 fold increase or decrease in mRNA transcripts was taken as a significant change. The expression of five genes (MMP-1, MMP-2, MMP-9, TIMP-2, sPLA2) was quantified for their respective abundance. Stimulation of normal rabbit synovial fibroblasts (SF) with IL-1β did not result in a significant (i.e., <1.5-fold) change in any of the mRNA levels examined, either with or without the peptide treatment. In contrast, mRNA expression of MMP1 (3.4 fold), MMP2 (2.1 fold), MMP9 (2.13 fold), and sPLA2 (2.73 fold) were significantly (>1.5 fold) elevated in IL-1β-stimulated human RASF, except for TIMP-2 mRNA which was down-regulated, but the level was not significant (−1.23 fold). Comparison of the results between the **10f**-treated and untreated SFs indicates that significant inhibition of gene expression was evident in both rabbit SF and human RASF for MMP-1, -2, and -9 and sPLA2 but not for TIMP-2.

Gelatin Zymography. To find out if this suppressive effect of the peptide on MMP gene expression is related to its direct inhibitory action on the catalytic activity, **10f** was examined for inhibition against the activity of gelatinases (MMP-2 and MMP-9) (Figure 10). Gelatin zymography of the concentrated supernatants collected from the cultures that were either untreated (IL-1β alone) or treated with 1-10 μM of peptide (IL-1β+ **10f**) showed that increasing doses of **10f** failed to show significant inhibition of MMP-2 and MMP-9 gelatinolytic activity (Figure 10A). Densitometric analysis of the zymograms (Figure 10B) confirmed that the activity of secreted MMP-2 and MMP-9 in culture media was not significantly reduced by varying doses (1−10 μM) of the peptide **10f** as compared to the untreated controls.

Discussion

Screening of Peptide Analogues. In the present study, we found that the peptide **10f**, containing two tandem repeats of **10**, resulted in significant enhancement in $sPLA_2$ inhibitory activity (IC_{50} 1.19 μM). The fact that the peptide with two copies of the core segment more effectively inhibited human synovial sPLA2 than the one containing a single copy segment should suggest that multiple copies of active pharmacophore sequence are an efficient method to increase the inhibition potency. The unique system of using multiple copies of drugs, peptides, or other active components has been proposed, and a multicomponent prodrug containing three copies of the targeting peptide and drug has been shown to have substantial enhancement in antitumor activity than the analogous prodrug containing one copy of active component.[23]

Solution Structure of Peptide Analogues. Detailed NMR and molecular modeling studies indicated that peptides **10** and **1** exhibited a β-turn structure in solution (Figures 3−5). A clear correlation between conformation of the peptides and *in vitro* activity was found among the four peptides studied. Peptides **1**, **10**, and **10f** exhibited secondary structure in solution and showed potent inhibitory activity, whereas the cyclic peptide **10e** that was devoid of any secondary structure did not have evidence of inhibitory activity. To understand the biological activity of the peptides, at least partial information on the 3D structure of a pharmacophore is essential. In the case of cyclic peptide **10e**, cyclization abolished the activity of the peptide although such cyclic peptide analogues are expected to improve the potency of the inhibition and binding of the peptide to sPLA2-IIA.[24] Judging from the structural information gained for **1**, **10**, and **10f** peptides, the β-turn around Trp-Asp-Gly-Val seems to play an important role. Surprisingly, the cyclic peptide **10e** did not show potent inhibitory activity and stable secondary structure. This may be due to flexibility of the cyclic structure of the peptide designed. Smaller cyclic peptides are known to exhibit stable secondary structure, while larger cyclic peptides exhibit flexible structure and may result in loss of activity. For cyclic peptides, optimum ring size[25] and the position of residues to impose a β-turn structure in the cyclic structure seems to be important. Among the three peptides (**1**, **10**, and **10f**), **10f** exhibited stable secondary structure and hence showed the highest inhibitory activity of 1.19 μM (IC_{50}). This may be due to the presence of two pharmacophores (Trp6-Asp7-Gly8-Va9l and Trp15-Asp16-Gly17-Val18) in the peptide, placed in proper orientation in a β-turn structure within the β-sheet. The peptide **10f** becomes a gel-like substance at a concentration ≥1 mM which clearly indicates that the β-sheet structure with a hydrophobic surface aggregates in water. The β-sheet nature of the peptide was also supported by CD spectra of peptide **10f** (a negative band around 217 nm, Figure 2).

Molecular Modeling. Docking studies were carried out to find the possible interaction of peptides with the sPLA2 receptor. Results of the docking studies were used to support the biological data. On the basis of the low energy docked

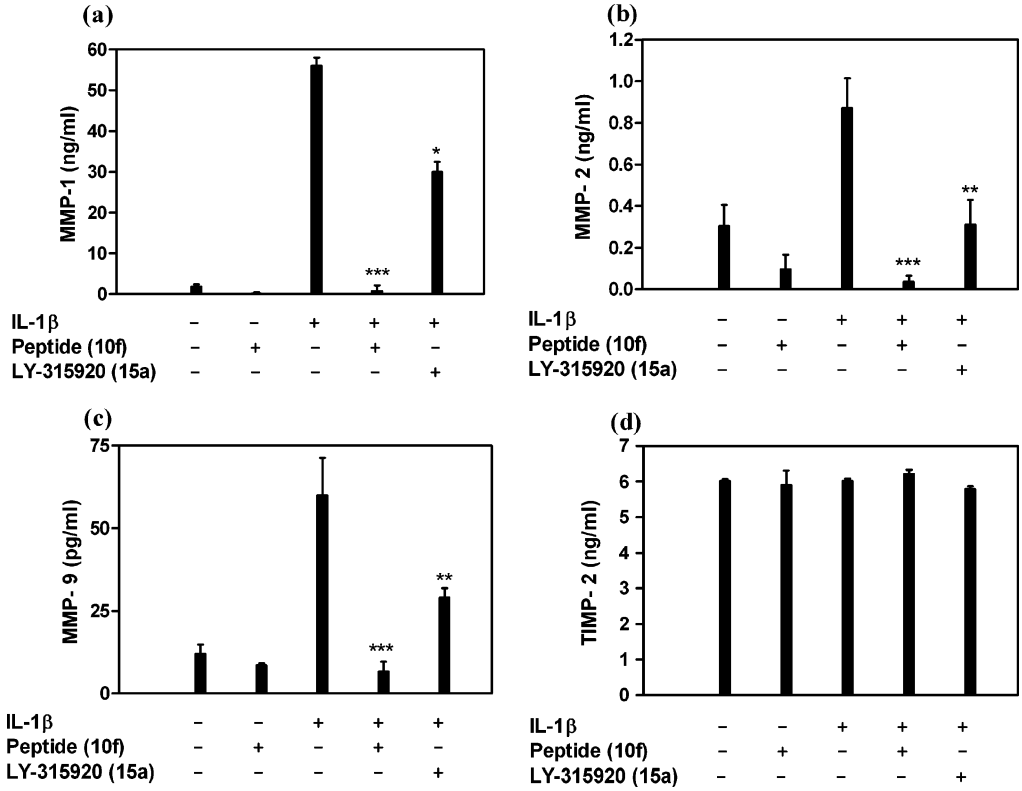

Figure 8. Inhibition of IL-induced MMP production by RASFs. (A) MMP-1, ((B) MMP-2, (C) MMP-9. In contrast to the suppressive effect of peptide **10f** or **15a** on MMP generation, none of the inhibitors had any effect on TIMP-2 (D) production by IL-stimulated RASFs.

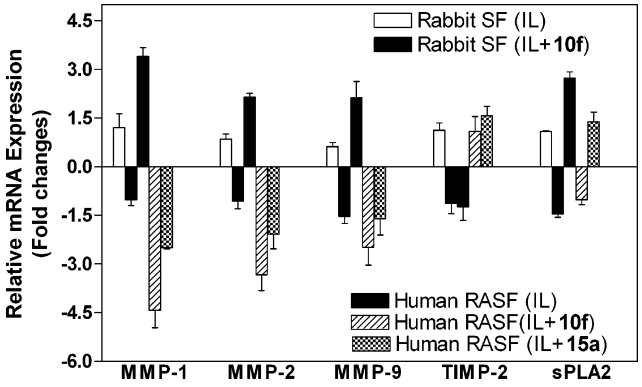

Figure 9. The effect of peptide on the relative expression of MMP and sPLA2 genes. QRT-PCR was used for assessing relative mRNA expression levels of IL-1β-stimulated rabbit FLSC and human RASF in the presence and absence of peptide **10f**. The relative levels of gene expression (mean ± SE) were normalized to the housekeeping gene (GAPDH). Cotreatment with the peptide significantly inhibited the IL-1β-induced expression of MMP-1, MMP-2, MMP-9, and sPLA2 genes from the cultured human RASFs and rabbit FLSCs.

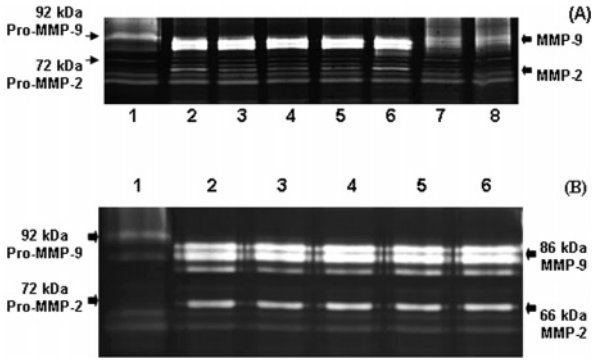

Figure 10. The effect of inhibitors on gelatinase (MMP-9 and MMP-2) activity in the supernatant of cultured rabbit synoviocytes (HIG-82). Supernatants from cells induced with IL-1β (5 ng) for 48 h was analyzed by gelatin zymography. (A) Supernatants (+1 mM APMA at 30 °C for 30 min) were preincubated with various inhibitors (5 μM peptides or 1−2 μM Calbiochem MMP inhibitor II) for 1 h at 25 °C prior to zymographic analyses: Lane 1, without activation (no inhibitor); Lane 2, with activation (no inhibitor); Lanes 3−8, with activation plus inhibitor: 3, peptide **1**; 4, peptide **10**; 5 and 6, peptide **10f**; 7 and 8, positive control MMP Inhibitor II (Calbiochem) at 1 and 2 μM concentrations. (B) Rabbit synovial fibroblasts were stimulated by IL-1β in the presence or absence of 1−10 μM of **10f** for 48 h. Concentrated culture supernatants (Centricon centrifugal filter devices, MW cutoff 30 000) were activated with APMA (1 mM final) before measurement of gelatinase activity by gelatin zymography. Lanes: 1 (−peptide − APMA); 2 (−peptide + APMA); 3 (+1 μM peptide + APMA); 4 (+5 μM peptide + APMA); 5 (+7.5 μM peptide + APMA); 6 (+10 μM peptide + APMA).

conformations of the peptides, **10** and **10f** have β-turn residues (Trp-Asp-Gly-Val) near the N-terminal region of the sPLA2 hydrophobic pocket, while the peptide **1** does not have such β-turn residues near the binding pocket. This is in correlation with the inhibitory activity of the peptides where **10** showed better inhibitory activity than **1**. The peptide **10f**, on the other hand, displayed two modes of binding with almost similar docked energy (−4.5 and −4 kcal/mol). It is a multimeric (dimeric) version of the peptide **10** with two pharmacophores, one at Trp6-Asp7-Gly8-Val9 and another at Trp15-Asp16-Gly17-Val18. Compared to peptides **1** and **10**, **10f** showed highest inhibitory activity with an IC_{50} of 1.19 μM. Introduction of two pharmacophores increased the potency of binding to sPLA2 or increased the effective concentration of the pharmacophore. It is also possible that the β-turn regions of the dimeric peptide may bind to two molecules of sPLA2, thus potentially

Table 4. Primer Sequences Used in Quantitative Real-Time PCR Analysis of Human RASF and Rabbit FLSC

gene name	forward primer (5′-3′)	reverse primer (5′-3′)	annealing temp (°C)	product size (bp)
human				
MMP-1	acagcttcccagcgactcta	cagggtttcagcatctggtt	58	200
MMP-2	ttgacggtaaggacggactc	acttgcagtactccccatcg	60	153
MMP-9	ctcgaactttgacagcgaca	ccctcagtgaagcggtacat	58	156
TIMP-2	gatgcacatcaccctctgtg	gtgcccgttgatgttcttct	55	196
$sPLA_2$ -IIA	aaggaagccgcactcagtta	ggcagcagccttatcacact	*56*	*243*
rabbit				
MMP-1	gacctgtcaagggcagatgt	caggtccatcaaagggagaa	57	163
MMP-2	ccccccaaaacggacaaagag	cacgagcaaaggcatcatcc	59	315
MMP-9	aaactggatgacgatgtctgcgtccc	acctgttccgctatggttacacccgcgt	57	362
TIMP-2	ggtagtgatccagggccaaag	attctctgtgacccagtccat	56	461
$sPLA_2$ -IIA	atcccatccaagagagctgac	tgtttccggcaggagtcctg	*57*	*326*
housekeeping				
β-actin	tcatgaagtgacgttgacatccgt	tcatgaagtgacgttgacatccgt	60	285
GAPDH	caaggtcatccacgaccact	ccagtgagtttcccgttcag	58	207

increasing the inhibitory activity. If we compare the docking energy of the peptides with the sPLA2 protein, peptide **1** had the lowest docked energy of −13.3 kcal/mol, followed by peptide **10** with −8 kcal/mol and peptide **10f** with −4 kcal/mol. These docked energies cannot be correlated with the activity of the peptides. The final docked energy depends on the total number of atoms used in the docking studies. The docking has a limitation depending on the size of the system used, the flexibility of the side chains considered, and the number of trial runs performed to achieve the lowest energy docking. A larger system may need more trials and extensive computer time.[26] Since the peptides used in the present study (**1**, **10**, **10f**) are varied in size, a direct correlation of docked energy of the peptides with inhibition activity may not be possible.

sPLA2−Peptide Binding. Previous studies have indicated that sPLA2 isoforms release arachidonic acid by cleavage of plasma membrane phospholipids.[22,27] Crystal structures of sPLA2 with different inhibitors[28,29] have indicated a conserved active site of the enzyme within a hydrophobic channel near the N-terminal helix of the protein. The hydrophobic channel is formed by Y51, K62, L2, F5, I19, A17, Y21, F98, and V30 (L2, F5, I9, I19, Y22, F106 in the case of snake venom sPLA2). This hydrophobic channel binds a single phospholipid molecule followed by interfacial binding of the enzyme to the aggregated phospholipid surface. Potent inhibitors bind to the hydrophobic channel, thus preventing the binding. The channel also has an enzyme active site in its rim with important residues H47 and D48.[22] Our docking studies of the sPLA2 crystal structure with peptide **10** and **10f** suggested that the β-turn residues of the peptides block the hydrophobic channel by binding to the hydrophobic pocket. Comparison of the crystal structure of the complex of one of the potent inhibitory peptides of snake PLA2, Phe-Leu-Ser-Tyr-Lys in complex with sPLA2 (snake venom),[30] indicated that peptides in our docking studies bind to the hydrophobic binding pocket near the N-terminal helix of sPLA2. Another potent small molecule inhibitor indole binding site[22] could be compared to the binding site of our peptides. Thus, it is reasonable to assume that the docking studies presented here give an overall view of interaction of peptides with protein sPLA2. On the basis of our NMR, docking, and inhibitory activity results, we can conclude that the β-turn residues Trp-Asp-Gly-Val are important in binding to sPLA2.

Gene and Protein Expression. IL-1, one of the key mediators involved in RA pathogenesis, is readily detected in the synovial fluid of patients with RA[31] and is known to affect gene expression levels in various settings.[32] In this study, we showed that IL-1β stimulation of the RASFs could significantly alter the expression of various genes involved in the pathophysiology of RA, including sPLA2 and matrix-modifying enzymes (MMP-1, MMP-3, MMP-2, MMP-9). The synovium is a site of increased expression of $sPLA_2$ in both RA and OA, and its presence in the fibroblast-like cells of RA synovial tissue indicates that the enzyme is specifically induced in these regions. The significant increase in gene and protein expression of $sPLA_2$ seen here in the IL-1-stimulated human RASFs, but not in the IL-1β-induced normal rabbit FLSC, suggests that sPLA2 is likely to play a significant part in synovial pathology. In several cell types, including primary rheumatoid synovial fibroblasts, overexpression of sPLA2s augments cyclooxygenase-2 (COX-2) induction and contributes to amplification of PGE2 production.[33−36] sPLA2 inhibitors can therefore contribute to amelioration of arthritic inflammation by suppressing PGE2 production in synovial cells. We have previously shown that the sPLA2 inhibitory peptide PN-T.II (coded PIP-17, **1** in this paper) and the specific and selective inhibitor of the group IIA sPLA2, **15a**,[37] suppressed TNF-induced release of prostaglandin E2 from cultured macrophage cells and suggest that the peptide may influence the prostaglandin-mediated inflammatory response in RASF by limiting the bioavailability of arachidonic acid through sPLA2 inhibition.[15]

Interestingly, the peptide inhibitor **10f** that we have designed appears not only to bind sPLA2 and inhibit its function but also downregulates the mRNA of sPLA2 and MMPs in our cytokine-induced RASF cell-based assays. Several proinflammatory cytokines (such as IL-1, IL-6, and TNF-a) induce transcription of the type IIA sPLA2 gene followed by eicosanoid generation in a wide variety of cells.[38,39] Transcriptional factors, including NFκB, PPAR, C/EBP, are known to play a role in the regulation of sPLA2 IIA gene expression.[40] However, the exact molecular mechanisms underlying downregulation of sPLA2 gene expression by sPLA2 inhibitors are yet to be clearly understood. Recent study on the role of PPARα in the induction of $sPLA_2$-IIA transcription by cytokines in rat mesangial cells indicates that $sPLA_2$-IIA released by the cells after treatment with cytokines potentiates its own gene expression in a positive feedback loop via activation of $cPLA_2$ and PPARα.[41] It has recently been reported that cytokine-induced $sPLA_2$-IIA gene expression is attenuated by the $sPLA_2$-IIA inhibitors, LY311727 (**15b**),[42] and Me-indoxam.[43] These findings suggest that the $sPLA_2$-IIA activity may be important for the enhanced expression of rat $sPLA_2$-IIA mRNA. Hence, it appears that the peptide **10f** suppresses mRNA expression of sPLA2 by inhibiting the catalytic activity, thereby interfering with the transcriptional

mechanism that enhances its gene expression in our cell-based experiments. On the basis of fold changes in sPLA2 mRNA and protein expression found after cytokine induction of RASFs with and without **10f** treatment, we estimated that the relative contribution of the peptide in the downregulation of $sPLA_2$-IIA accounts for about 60% for the protein, and 40% for mRNA. This means that the sPLA2-IIA protein inhibition by the peptide may be relatively more important than its effect on gene expression, at least in this model of human RASF cells. Nevertheless, the peptide that can interfere with sPLA2-induced activation of inflammatory cells through inhibition of enzymatic and transcriptional activity may likely be more beneficial for therapeutic use.

In addition to the increased sPLA2 expression, the gene as well as protein expression levels of MMP-1, MMP-2 and MMP-9 were found to be significantly increased in our IL-1β-stimulated cultured human RASFs but not in the IL-stimulated normal rabbit FLSCs. The suppressive effect on MMP transcription unexpectedly found in our study with PLA2 inhibitors such as peptides **10f** and **15a** may likely be due to their interference on transcription factors. The AP-1 site upstream of the transcriptional start site has been thought to play a critical role in the transcriptional activation of MMP gene.[44] Activation of p38 and JNK MAPK is commonly responsible for AP-1 activation through the phosphorylation of c-Jun.[45] The involvement of MAPK cascades has been demonstrated for the regulation of MMP expression.[46,47] We have found that pretreatment of RASF with the peptide **10f** effectively blocks p38 phosphorylation, while IL-1-induced ERK phosphorylation was only partially inhibited by peptide treatment (manuscript in preparation). Although the detailed inhibitory mechanism is not yet determined, it is possible that the suppressive effect of peptide **10f** on MMP mRNA expression is likely to be mediated by an inhibition of p38 MAPK, which is necessary for induction of MMP transcription.

Cultured cells such as RASFs respond to proinflammatory cytokines such as IL-1β with the production of several MMP proteins, mainly due to an increase in gene transcription. Overproduction of MMP mediates the irreversible cartilage degradation and joint destruction of RA.[48] It is conceivable that the suppressive effect of the peptide on MMP mRNA transcription will lead to reduced production of MMPs in the cultured medium, thus resulting in reduced cartilage degradation and joint destruction in RA.

Other than suppressing MMP protein production via its effect on the gene expression, the peptide may also inhibit MMP protein expression probably through its inhibitory action on sPLA2 expression. sPLA2s participate in inflammation reactions by mobilizing free fatty acids including arachidonic acid, and thus initiating the metabolic cascade leading to the biosynthesis of lipid mediators (e.g., prostaglandins). Prostaglandins (PG), especially PGE_1 and PGE_2, have been reported to upregulate the production of MMPs in synoviocytes.[49] Human prostate tumor cells that received the PLA2 inhibitor 4-bromophenacyl bromide (4-BPB) showed a significant reduction in the levels of proMMP-2, MMP-9, and proMMP-9 in the culture medium.[50] This concerted inhibition of cytokine-induced sPLA2 and MMP expressions strongly suggests that the modulatory action of the peptide may play a major role in counteracting the development of inflammatory arthritis. Our recent *in vivo* study (manuscript in preparation) has, in fact, demonstrated that the dimeric peptide **10f** significantly decreased synovial inflammation and cartilage and bone erosion in a transgenic mouse model of inflammation.[15]

Conclusions. We report here for the first time the activity of a dual sPLA2/MMP inhibitor proven in primary synovium cultures from RA patients. The peptide inhibitor was identified through screening of a family of peptide analogues by enzyme assays, followed by cell-based experiments, and by gene and protein expression analyses. A model for the peptide−protein interaction was proposed based on NMR and molecular modeling studies. It contains two pharmacophores with each having a β-turn structure at Trp-Asp-Gly-Val residues that is important in binding to the hydrophobic channel of the sPLA2 protein. The dual inhibitor potently inhibits IL-1β-induced secretions of sPLA2 and MMPs (MMP-1, -2, -3, and -9) both at protein and mRNA levels but did not inhibit protein and mRNA levels of natural endogenous inhibitors (TIMPs). Since both sPLA2 and MMPs have been proposed to play a significant role in RA etiology, a dual inhibitor such as this peptide may be effective and beneficial for treatment of RA.

Experimental Section

Chemistry. Sterile Dulbecco's Modified Eagle's Medium (DMEM) and Ham's F-12-K medium were purchased from the National University Medical Institute (NUMI) stores, Singapore, and American Type Culture Collection (Manassas, VA), respectively. Cell culture grade antibiotic mixture of penicillin−streptomycin solution (10 000 units mL^{-1} penicillin, 10 000μg mL^{-1} streptomycin in 0.85% saline) was purchased from Gibco-BRL products (Gaithersburg, MD). Tissue culture grade trypsin−EDTA solution (5.0 g of porcine trypsin and 2.0 g of EDTA in 0.9% saline), 4-aminophenylmercuric acetate (APMA), dimethyl sulfoxide (DMSO), and deuterated dimethyl sulfoxide-d_6 (DMSO-d_6) were from Sigma-Aldrich (St. Louis, MO). Collagenase II was from Worthington Biochemical Corporation, Lakewood, NJ, and recombinant human interleukin 1β was from Chemicon, Temecula, CA. An organic indole analogue **15a** was a gift from Lilly Research Laboratories, Indianapolis, IN. All other chemicals and reagents used were purchased from NUMI stores, Singapore.

Synthesis and Characterization of sPLA2 Inhibitory Peptides. A family of linear peptide analogues (Table 1) was synthesized based on the sequence of PIP[12] (GenBank Accession nos. AAF73945, AX175043, CAC43861, CAC43862, and CAC43863) using the solid-phase method with 9-fluorenylmethoxycarbonyl chemistry. The peptides were purified by successive chromatography with gel filtration and reverse phase high-pressure liquid chromatography to more than 95% purity. The sequences were validated by matrix-assisted laser desorption/ionization time-of-flight mass spectrometry (MALDI-TOF−MS). The linear and cyclic peptides used for NMR were designed and custom synthesized. **1**, **10**, and **10e** peptides were synthesized at Mimotopes (Clayton, Victoria, Australia), while the main peptide **10f** was synthesized at AnaSpec, Inc. (San Jose, CA). The pure products were analyzed by HPLC and MS. The HPLC chromatogram showed that the purities of peptides were more than 95%, and MS showed the correct molecular ion for the peptides (Table S1 in Supporting Information).

Determination of sPLA2 Inhibitory Activity. This was carried out as previously described.[11] In brief, [^{3}H]arachidonate-labeled *E. coli* membranes (0.005 mCi/mL; 5.8μCi/μmol, NEN, PerkinElmer Life Sciences, Inc., Boston, MA) were used as substrate, and 100 mM Tris-HCl, 25 mM $CaCl_2$, pH 7.5 solution as an assay buffer. The reaction mixture contained 20 μL of substrate, 0.85 pmol of purified human synovial $sPLA_2$ (human Type IIA $sPLA_2$, Cayman Chemicals, Ann Arbor, MI), and increasing concentrations of the family of synthetic peptides derived from the sequence of PIP. The amount of [^{3}H]-labeled arachidonate released from the *E. coli* membrane was measured using liquid scintillation counting (Multipurpose Scintillation Counter LS 6500; Beckman, Fullerton, CA). As controls, $sPLA_2$ was preincubated with the assay buffer alone. All samples, including controls, were performed in triplicate and plotted as the percentage inhibition relative to negative controls. Peptides were evaluated relative to a positive control synthetic

peptide **1** and a negative control peptide **2**, i.e, scrambled peptide of **1**, included in each assay.

IC_{50} Determination. IC_{50} was determined by preincubating varying concentrations (1−250 M) of inhibitors in a constant volume, against a constant amount of enzyme as described earlier. A sigmoid dose−response curve was generated to allow calculation of the IC_{50} values. All samples were performed in triplicate. Results were analyzed by nonlinear regression with GraphPad Prism (version 4.01) and expressed as the percentage of inhibition relative to control values.

Cell Cultures. HIG-82 rabbit FLSC cell line obtained from American Type Culture Collection (Manassas, VA; catalog No.CRL-1832) was used as a nonarthritis control. Human RASF were prepared from the primary cultures of fresh synovial tissue samples taken from three active RA patients at total knee-replacement surgery according to the clinical criteria of the American Rheumatism Association. Minced RA synovial tissue samples were treated with 1 mg/mL collagenase for 20 min at 37 °C and grown under standard conditions (37 °C/5% CO_2) in DMEM supplemented with 10% FBS, 100 U/mL of penicillin, and 100 mg/mL of streptomycin. Following trypsinization, the harvested cells were propagated in 75-cm^2 flasks until reaching passage 3. Only RASF passages 3−8 were used in experiments to ensure that cultures would be free of contaminating macrophages. For experiments, RASFs seeded in 75-cm^2 flasks were allowed to reach confluence and serum-starved for overnight (16 h). Three different doses (1, 5, 10 μM) of peptide **10f** were examined to find the peptide concentration that showed maximal inhibitory effect on IL-1β-induced sPLA2 production. To investigate whether sPLA2 inhibitors have a modulatory effect on the sPLA2 and MMP mRNA expression, RASFs were preincubated for 1 h with 5 μM **10f** or **15a** or with vehicle (0.1% DMSO final concentration in medium) and then stimulated with hrIL-1β (10 ng/mL) for 24 h. RASF cultured without IL-1β or the peptide served as controls.

Control rabbit normal FLSC were grown under standard conditions (37 °C/5% CO_2) in Ham's F-12 medium containing 10% fetal bovine serum (FBS) and 1% penicillin/streptomycin, as recommended by the supplier. Subcultured FLSC seeded at 10^5/well were then grown to 80% confluence on 12-well culture dishes and starved in a serum-free medium with or without 5 μM **10f** for 2 h. Control cultures received equivalent additions of either medium or medium containing vehicle (0.1% DMSO). The cells were then stimulated with 5 ng/mL rhIL-1 β for 24 h and collected for RNA extraction after washing with cold PBS.

Measurement of sPLA2 and MMP Proteins. Above RASF samples were centrifuged briefly, and supernatants were stored at −20 °C until use for determination of the expressed levels of sPLA2 and MMP proteins. ELISA kits for triplicate sample determinations of sPLA2 (sPLA2 human type IIA EIA kit, Catalog No.585000) and MMPs (ELISA kits for human MMP-1, MMP-2, MMP-3, and MMP-9) were from Cayman Chemical Co., and RayBiotech, Inc., Norcross, GA, respectively.

Gelatin Zymography. Culture supernatants collected and stored at −20 °C were thawed on ice and concentrated by centrifugation in Centricon centrifugal filter devices (MW cutoff 30 000) for 35 min at 5000 rpm at 4 °C. After activation with APMA (1 mM final concentration), the samples were measured for gelatinase (MMP-2 and -9) activity by gelatin zymography. Human synovial fluid, purified human recombinant MMP-2 and -9 (as standard markers), or APMA-activated concentrated culture supernatant samples (10 uL) was mixed (1:1) with Laemmli sample buffer, loaded on 4% acrylamide stacking gel, and electrophoresed (120 V) at 4 °C on a 10% acrylamide-resolving minigel containing 0.1% gelatin. After electrophoresis for 1 h, the gels were soaked in 2.5% Triton X-100 on a shaker for 1 h, changing the solution after 30 min, to eliminate SDS. After overnight incubation in zymogen activation buffer [50 mM Tris-HCl, pH 7.5, containing 10 mM $CaCl_2$ and 5 mM $ZnCl_2$] at 37 °C, the gels were rinsed in distilled water and stained for 3 h with Bromphenol blue, after which clear bands of digested gelatin were clearly visible. The gels were briefly rinsed in distilled water and scanned by the Bio-Rad GS-710 calibrated imaging densitometer.

Cell Viability Assays. XTT (sodium 3′-[phenylaminecarboxyl]-3,4-tetrazolium]-bis(4-methoxynitrobenzene sulfonic acid hydrate)) Cell Proliferation Kit II (Roche Applied Science) was used to assess the possible cytoxic effect of the peptides on the rabbit FLSC and human RASF.

RNA Extraction and Quantitative Real Time RT-PCR. After removal of supernatants for protein assays, the remaining RASF cells were washed with cold PBS and pooled ($n = 3$ flasks) for each group [controls (− IL-1β), IL-1β only, IL-1β + **10f**, IL-1β + **15a**]. Total RNA was isolated using RNeasy mini kit (Qiagen, Inc., Valencia, CA), subsequently treated with RNase-free Dnase-I (Qiagen) at room temperature for 20 min and stored at −80 °C until use. The quality and quantity of extracted RNA was determined by spectrophotometry (Bio-Rad Laboratories, Hercules, CA). All RNA samples used for qRT-PCR experiments were of highest purity with A_{260}/A_{280} ratios of 1.9-2.1. Reverse Transcription (RT) of RNA, amplification, detection of DNA, data acquisition, and subsequent qRT-PCR analysis were performed as described previously.[51] The sense and antisense primers used for specific amplification and conditions for PCR cycles are shown in Table 4. The primers were designed by Primer3 software: http://bioinformatics. weizmann.ac.il/cgi-bin/primer/primer3.cgi and subsequently checked for specificity using BLAST: http://www.ncbi.nlm.nih.gov/genome/seq/HsBlast.html. All primers were synthesized by first BASE Pvt. Ltd., Singapore. The expression of *GAPDH* was used as an internal calibrator for equal RNA loading and to normalize relative expression data for all other genes analyzed. The real-time RT-PCR data were quantified using relative quantification ($2^{-\Delta\Delta C}$T) method as described.[52]

NMR Spectroscopy. Since the peptides **1**, **10**, and **10f** were not soluble in water at the concentration needed for NMR studies, two solvent systems: 50% water and 50% deuterated dimethyl sulfoxide and 100% deuterated dimethyl sulfoxide, were used for sample preparation. Each peptide (3−5 mg) was dissolved either directly in 0.5 mL of 100% or dissolved first in 0.25 mL of DMSO followed by addition of 0.25 mL of water later. The temperature dependence of the amide proton chemical shift was measured by collecting data from 293 K to 313 K in steps of 5 K using a variable temperature probe. The one- and two-dimensional NMR experiments were performed and processed on 500 and 800 MHz Bruker NMR spectrometers equipped with a 5-mm broad-band inverse probe, at a proton frequency of 500.13 and 800.15 MHz, respectively. Spectra were acquired at 298 K unless otherwise specified. TOCSY,[53] DQF-COSY,[54] rotating frame nuclear Overhauser spectroscopy (ROESY),[55] and NOESY[56] experiments were performed by presaturation of water during relaxation delay or by gradient suppression of water signal.[57] Data were collected by the TPPI method[58] with a sweep width of 5000 Hz. Spectra were processed using XWINNMR and TOPSPIN softwares (Bruker, Inc.). Analysis of the data and assignments of the resonance were carried out using Sparky software.[59] ROE cross-peak volumes for peptides were measured using ROESY spectra with 200−300 ms spin-lock times, and NOESY cross-peak volumes were measured at 200 ms mixing time. Cross-peak volumes and chemical shifts were saved in DYANA format and used for further calculations. Coupling constants ($^3J_{HN\alpha}$) were measured from the DQF-COSY spectrum and well resolved 1D NMR spectrum.

Determination of Peptide Structures. Conformational space was searched for the peptides using CYANA[60,61] and InsightII software version 2000 (Accelrys Inc., San Diego, CA) to identify conformations consistent with the experimental ROE/NOE and coupling constant data.[62] Briefly, structures were generated using distance geometry-based algorithms with NMR constraints using CYANA. Side chain protons were not stereospecifically assigned; hence, ROE/NOE restraints for the side-chain protons were calculated by considering pseudo atoms.[18] A total of 100 structures were generated, and these were subjected to the simulated annealing

procedure. Twenty structures that have a low target function[60,61] were selected for further calculations. The target function takes into account ROE/NOE violations, peptide bond lengths, and bond angle restraints. The structures were checked for the quality using a Ramachandran map and InsightII (bond length, bond angle, and peptide bond torsion angle). An average structure was chosen from this family as a representative structure.

Docking. Complexes of peptide−PLA2 protein were generated by docking of **1**, **10**, and **10f** peptides to the PLA2 protein crystal structure. All docking studies were performed with the autodock program[63] (version 3.0). To search the low energy docked conformation of the ligand (i.e., peptide inhibitor) on the receptor (i.e., sPLA2 enzyme), the Lamarckian genetic algorithm approach available in the autodock software was used. In this approach, the ligand performs a random walk around the static protein. At each time step, the ligand is moved by small increments in global translation and orientation at each of the rotational torsion angles. Depending on the input parameter values for the number of generations and the total number of energy evaluations, configurations are generated for grid points on the protein surface. The energy of the configurations is calculated based on a previously defined grid surface. Interaction energies are calculated with a free-energy-based expression. The docked energies are listed in the increasing order of energy.

The coordinates of peptides were retrieved from the NMR-determined structure (studies presented in this paper), and the coordinates of ligated PLA2 were retrieved from the Protein Data Bank (accession code 1DCY; the protein was unmerged from the complex of protein and ligand).[22] Water molecules and ions were removed. For the protein receptor, polar hydrogens were added and kollman charges were assigned. For the peptide molecules, all the hydrogens were used with kollman charges. Docking simulations were carried out on a PC with redhat linux 9.0. In the autodock, grids were calculated with 128 elements ($128 \times 128 \times 128$) with a grid spacing of 0.375 Å. The center of the grid was chosen at the C_α atom F5 of the protein. Previous studies[24] have shown that the N-terminal part of sPLA2 consists of the binding site which is formed by L2, F5, and I9. Thus, it was reasonable to choose the C_α atom of F5 as the grid center in the docking studies. Lennard−Jones parameters 12−10 and 12−6 were used for modeling H-bonds and Van der Waals interactions, respectively. The distance-dependent dielectric permittivity was used for the calculation of electrostatic grid maps. The torsion angles of the side chains of the ligand peptide were set to rotate using flexible docking. Peptide bonds were held constant. The protein (receptor) atoms were not allowed to move during the docking. Docking studies were carried out using the Lamarckian Genetic algorithm (LGA) option available in autodock 3.0. Pseudo-Solis and Wets methods were applied for minimization in the autodock software. The size of the population was set to 50 in GA runs. The rate of gene mutation and the rate of gene crossover were set to 0.02 and 0.08, respectively. The number of energy evaluations was set to 1.5 million. After docking, all structures generated for the peptides were assigned to clusters based on a tolerance of 1.0 Å all-atom rmsd from the lowest-energy structure. The docked conformations of the ligand peptide were listed in increasing energy order, and ligand conformation with lowest energy was used as reference for each starting position of docking. Final possible docked structures were selected based on the docking energy values. The docked structures were analyzed using autodock tools for hydrogen bonding and hydrophobic interactions.

Circular Dichroism (CD) Measurement. CD experiments were carried out at room temperature on a Jasco J-810 spectropolarimeter flushed with nitrogen. Spectra were collected from 240 to 190 nm using 1 mm path length of cylindrical quartz cell. Each spectrum was an average of three scans taken at a scan rate of 50 nm/min with a spectral bandwidth of 1 nm. Peptide was dissolved in 10 μL of DMSO first and then diluted to the desired concentration by adding water. The final concentration of peptide was 0.15 mM. For the final representation, the baseline was subtracted from the spectrum, and the spectra were represented as ellipticity in mdeg. CD spectra were analyzed and assigned to secondary structure such as β-turn, β-sheet, or open conformation by comparing the spectra to the CD spectra available in the literature.[16]

Statistical Analysis. Unless otherwise indicated, the anova single factor test was used to evaluate group means of continuous variables. If the anova single factor test was significant, a *post hoc* test was done using Dunnet's multiple comparison test. Analyses were performed using Prism statistical software (GraphPad Prism version 4.01, GraphPad Software Inc., San Diego, CA).

PDB Deposit Information. Twenty low-energy structures of peptides **1** (PIP-17), **10** (PIP-9), and **10f** (PIP-18) were deposited in the protein data bank along with NMR chemical shifts values (PDB ID codes, PIP-9, 2P5H; PIP-17, 2P5J; PIP-18, 2P60).

Acknowledgment. This research was funded by Research grant no. NMRC/CPG/013/2005; R-181-000-092-213) from the National Medical Research Council, Singapore. We would also like to thank Lilly Research Laboratories, Indianapolis, IN, for the kind gift of the research material **15a** for use in our enzyme assays.

Supporting Information Available: Analytical data for synthetic peptides studied in this work (Table 1), NMR chemical shift data for synthetic peptides (Tables 2−4) for PIP-9 (**10**), PIP-17 (**1**), and PIP-18 (**10f**) peptides, and 600 MHz TOCSY and NOESY/ROESY data for the peptides **10**, **1**, and **10f** (Figures 1−7). This material is available free of charge via the Internet at http://pubs.acs.org.

References

(1) Murakami, M.; Kudo, I. Phospholipase A2. *J. Biochem. (Tokyo*) **2002**, *131*, 285−292.
(2) Triggiani, M.; Granata, F.; Oriente, A.; Gentile, M.; Petraroli, A.; Balestrieri, B.; Marone, G. Secretory phospholipases A2 induce cytokine release from blood and synovial fluid monocytes. *Eur. J. Immunol.* **2002**, *32*, 67−76.
(3) Pruzanski, W.; Vadas, P. Phospholipase A2: a mediator between proximal and distal effectors of inflammation. *Immunol. Today* **1991**, *12*, 143−146.
(4) Jamal, O. S.; Conaghan, P. G.; Cunningham, A. M.; Brooks, P. M.; Munro, V. F.; Scott, K. F. Increased expression of human type IIa secretory phospholipase A2 antigen in arthritic synovium. *Ann. Rheum. Dis.* **1998**, *57*, 550−558.
(5) Pruzanski, W.; Keystone, E. C.; Sternby, B.; Bombardier, C.; Snow, K. M.; Vadas, P. Serum phospholipase A2 correlates with disease activity in rheumatoid arthritis. *J. Rheumatol.* **1988**, *15*, 1351−1355.
(6) Burrage, P. S.; Mix, K. S.; Brinckerhoff, C. E. Matrix metalloproteinases: role in arthritis. *Front Biosci.* **2006**, *11*, 529−543.
(7) Konttinen, Y. T.; Ainola, M.; Valleala, H.; Ma, J.; Ida, H.; Mandelin, J.; Kinne, R. W.; Santavirta, S.; Sorsa, T.; Lopez-Otin, C.; Takagi, M. Analysis of 16 different matrix metalloproteinases (MMP-1 to MMP-16) in the synovial membrane: different profiles in trauma and rheumatoid arthritis. *Ann. Rheum. Dis.* **1999**, *58*, 691−697.
(8) Borkakoti, N. Matrix metalloprotease inhibitors: design from structure. *Biochem. Soc. Trans.* **2004**, *32*, 17−20.
(9) Lee, C.; Lee, J.; Choi, Y. A.; Kang, S. S.; Baek, S. H. cAMP elevating agents suppress secretory phospholipase A(2)-induced matrix metalloproteinase-2 activation. *Biochem. Biophys. Res. Commun.* **2006**, *340*, 1278−1283.
(10) Pruzanski, W.; Stefanski, E.; Vadas, P.; McNamara, T. F.; Ramamurthy, N.; Golub, L. M. Chemically modified non-antimicrobial tetracyclines inhibit activity of phospholipases A2. *J. Rheumatol.* **1998**, *25*, 1807−1812.
(11) Uitto, V. J.; Firth, J. D.; Nip, L.; Golub, L. M. Doxycycline and chemically modified tetracyclines inhibit gelatinase A (MMP-2) gene expression in human skin keratinocytes. *Ann. N. Y. Acad. Sci.* **1994**, *732*, 140−151.
(12) Gu, Y.; Lee, H. M.; Golub, L. M.; Sorsa, T.; Konttinen, Y. T.; Simon, S. R. Inhibition of breast cancer cell extracellular matrix degradative activity by chemically modified tetracyclines. *Ann. Med.* **2005**, *37*, 450−460.

(13) Thwin, M. M.; Ong, W. Y.; Fong, C. W.; Sato, K.; Kodama, K.; Farooqui, A. A.; Gopalakrishnakone, P. Secretory phospholipase A2 activity in the normal and kainate injected rat brain, and inhibition by a peptide derived from python serum. *Exp. Brain Res*. **2003**, *150*, 427−433.
(14) Thwin, M. M.; Gopalakrishnakone, P.; Kini, R. M.; Armugam, A.; Jeyaseelan, K. Recombinant antitoxic and antiinflammatory factor from the nonvenomous snake Python reticulatus: phospholipase A2 inhibition and venom neutralizing potential. *Biochemistry* **2000**, *39*, 9604−9611.
(15) Thwin, M. M.; Douni, E.; Aidinis, V.; Kollias, G.; Kodama, K.; Sato, K.; Satish, R. L.; Mahendran, R.; Gopalakrishnakone, P. Effect of phospholipase A2 inhibitory peptide on inflammatory arthritis in a TNF transgenic mouse model: a time-course ultrastructural study. *Arthritis Res. Ther*. **2004**, *6*, R282−294.
(16) Perczel, A.; Fasman, G. D. Quantitative analysis of cyclic β-turn models. *Protein Sci.* **1992**, *1*, 378−395.
(17) Fasman, G. D. *Circular Dichroism and the Conformational Analysis of Biomolecules*; Plenum Press: New York, 1996.
(18) Wüthrich, K. *NMR of Proteins and Nucleic Acids*; John Wiley & Sons: New York, 1986.
(19) Anderson, N. H.; Neidigh, W. J.; Harris, N. S.; Lee, G. M.; Liu, Z.; Tong, H. Extracting Information from the Temperature Gradients of Polypeptide NH Chemical Shifts. 1. The Importance of Conformational Averaging. *J. Am. Chem. Soc.* **1997**, *119*, 8547−8561.
(20) Wishart, D. S.; Sykes, B. D.; Richards, F. M. The chemical shift index: a fast and simple method for the assignment of protein secondary structure through NMR spectroscopy. *Biochemistry* **1992**, *31*, 1647−1651.
(21) Rose, G. D.; Gierasch, L. M.; Smith, J. A. Turns in peptides and proteins. *Adv. Protein Chem.* **1985**, *37*, 1−97.
(22) Schevitz, R. W.; Bach, N. J.; Carlson, D. G.; Chirgadze, N. Y.; Clawson, R. D.; Dillard, S. E.; Draheim, S. E.; Hartley, L. W.; Jones, N. D.; Mihelich, E. D.; Olkowski, J. L.; Snyder, D. W.; Sommers, C.; Wery, J. P. Structure-based design of the first potent and selective inhibitor of human non-pancreatic secretory phospholipase A2. *Nature Struct. Biol*. **1995**, *2*, 458−465.
(23) Khandare, J. J.; Chandna, P.; Wang, Y.; Pozharov, V. P.; Minko, T. Novel polymeric prodrug with multivalent components for cancer therapy. *J. Pharmacol. Exp. Ther.* **2006**, *317*, 929−937.
(24) Church, W. B.; Inglis, S. A.; Tseng, A.; Duell, R.; Lei, P. W.; Bryant, K. J.; Scott, K. F. A novel approach to the design of inhibitors of human secreted phospholipase A2 based on native peptide inhibition. *J. Biol. Chem.* **2001**, *276*, 33156−33164.
(25) Hruby, V. J.; Al-Obeidi, F.; Kazmierski, W. Emerging approaches in the design of receptor-selective peptide ligands: conformational topographical and dynamic considerations. *Biochem. J.* **1990**, *268*, 249−262.
(26) Hetenyi, C.; Spoel, D. V. Efficient docking of peptides to proteins without prior knowledge of the binding site. *Protein Sci.* **2002**, *11*, 1729−1737.
(27) Bayburt, T.; Yu, B.-Z.; Lin, H.-K.; Browning, J.; Jain, M. K.; Gelb, M. H. Human nonpancreatic secreted phospholipase A2: interfacial parameters, substrate specificities, and competitive inhibitors. *Biochemistry* **1993**, *32*, 573−582.
(28) Dijkstra, B.; Kalk, K.; Hol, W.; Drenth, J. Structure of bovine pancreatic phospholipase A2 at 1.7A resolution. *J. Mol. Biol*. **1981**, *147*, 97−123.
(29) Scott, D. L.; Otwinowski, Z.; Gelb, M. H.; Sigler, P. B. Crystal structure of bee-venom phospholipase A2: correction. *Science* **1991**, *252*, 764.
(30) Chandra, V.; Jast, J.; Kaur, P.; Dey, S.; Perbandt, M.; Srinivasan, A.; Betzel, Ch.; Singh, T. P. Crystal structure of a complex formed between a snake venom phospholipase A2 and a potent peptide inhibitor Phe-Leu-Ser-Tyr-Lys at 1.8 Å resolution. *J. Biol. Chem.* **2002**, *277*, 41079−41085.
(31) Feldmann, M.; Brennan, F. M.; Maini, R. N. Role of cytokines in rheumatoid arthritis. *Annu. Rev. Immunol*. **1996**, *14*, 397−440.
(32) Jeong, J. G.; Kim, J. M.; Cho, H.; Hahn, W.; Yu, S. S.; Kim, S. Effects of IL-1beta on gene expression in human rheumatoid synovial fibroblasts. *Biochem. Biophys. Res. Commun.* **2004**, *324*, 3−7.
(33) Murakami, M.; Kambe, T.; Shimbara, S.; Higashino, K.; Hanasaki, K.; Arita, H.; Horiguchi, M.; Arita, M.; Arai, H.; Inoue, K. et al. Different functional aspects of the group II subfamily (types IIA and V) and type X secretory phospholipase A2s in regulating arachidonic acid release and prostaglandin generation: implication of cyclooxygenase-2 induction and phospholipid scramblase-mediated cellular membrane perturbation. *J. Biol. Chem.* **1999**, *274*, 31435−31444.
(34) Bidgood, M. J.; Jamal, O. S.; Cunningham, A. M.; Brooks, P. M.; Scott, K. F. Type IIA secretory phospholipase A2 up-regulates cyclooxygenase-2 and amplifies cytokine-mediated prostaglandin production in human rheumatoid synoviocytes. *J. Immunol.* **2000**, *165*, 2790−2797.
(35) Masuda, S.; Murakami, M.; Komiyama, K.; Ishihara, M.; Ishikawa, Y.; Ishii, T.; Kudo, I. Various secretory phospholipase A2 enzymes are expressed in rheumatoid arthritis and augment prostaglandin production in cultured synovial cells. *FEBS J*. **2005**, *272*, 655−672.
(36) Higashi, S.; Ohishi, H.; Kudo, I. Augmented prostaglandin E2 generation resulting from increased activities of cytosolic and secretory phospholipase A2 and induction of cyclooxygenase-2 in interleukin-1 beta-stimulated rat calvarial cells during the mineralizing phase. *Inflamm. Res.* **2000**, *49*, 102−111.
(37) Snyder, D. W.; Bach, N. J.; Dillard, R. D.; Draheim, S. E.; Carlson, D. G.; Fox, N.; Roehm, N. W.; Armstrong, C. T.; Chang, C. H.; Hartley, L. W.; Johnson, L. M.; Roman, C. R.; Smith, A. C.; Song, M.; Fleisch, J. H. Pharmacology of LY315920/S-5920, [[3-(aminooxoacetyl)-2-ethyl-1-(phenylmethyl)-1H-indol-4-yl]oxy] acetate, a potent and selective secretory phospholipase A2 inhibitor: A new class of anti-inflammatory drugs, SPI. *J. Pharmacol. Exp. Ther*. **1999**, *288*, 1117−1124.
(38) Schwemmer, M.; Aho, H.; Michel, J. B. Interleukin-1beta-induced type IIA secreted phospholipase A2 gene expression and extracellular activity in rat vascular endothelial cells. *Tissue Cell* **2001**, *33*, 233−240.
(39) Jacques, C.; Bériéziat, G.; Humbert, L.; Olivier, J. L.; Corvol, M. T.; Masliah, J.; Berenbaum, F. Posttranscriptional effect of insulin-like growth factor-I on interleukin-1beta-induced type II-secreted phospholipase A2 gene expression in rabbit articular chondrocytes. *J. Clin. Invest.* **1997**, *99*, 1864−1872.
(40) Touqui, L.; Alaoui-El-Azher, M. Mammalian secreted phospholipases A2 and their pathophysiological significance in inflammatory diseases. *Curr. Mol. Med*. **2001**, *1*, 739−754.
(41) Beck, S.; Lambeau, G.; Scholz-Pedretti, K.; Gelb, M. H.; Janssen, M. J.; Edwards, S. H.; Wilton, D. C.; Pfeilschifter, J.; Kaszkin, M. Potentiation of tumor necrosis factor alpha-induced secreted phospholipase A2(sPLA2)-IIA expression in mesangial cells by an autocrine loop involving sPLA2 and peroxisome proliferator-activated receptor alpha activation. *J. Biol. Chem.* **2003**, *278*, 29799−29812.
(42) Schevitz, R. W.; Bach, N. J.; Carlson, D. G.; Chirgadze, N. Y.; Clawson, D. K.; Dillard, R. D.; Draheim, S. E.; Hartley, L. W.; Jones, N. D; Mihelich, E.D.; *et al.* Structure-based design of the first potent and selective inhibitor of human non pancreatic secretory phospholipase A2. *Nat. Struct. Biol*. **1995**, *2*, 458−465.
(43) Smart, B. P.; Pan, Y. H.; Weeks, A. K.; Bollinger, J. G.; Bahnson, B. J.; Gelb, M. H. Inhibition of the complete set of mammalian secreted phospholipases A(2) by indole analogues: a structure-guided study. *Bioorg. Med. Chem.* **2004**, *12*, 1737−1749.
(44) Westermarck, J.; Kähäri, V. M. Regulation of matrix metalloproteinase expression in tumor invasion. *FASEB J.* **1999**, *13*, 781−792.
(45) Whitmarsh, A. J.; Davis, R. J. Transcription factor AP-1 regulation by mitogen-activated protein kinase signal transduction pathways. *J. Mol. Med.* **1996**, *74*, 589−607.
(46) Eberhardt, W.; Huwiler, A.; Beck, K. F.; Walpen, S.; Pfeilschifter, J. Amplification of IL-1 beta-induced matrix metalloproteinase-9 expression by superoxide in rat glomerular mesangial cells is mediated by increased activities of NF-kappa B and activating protein-1 and involves activation of the mitogen-activated protein kinase pathways. *J. Immunol.* **2000**, *165*, 5788−5797.
(47) Benelli, R.; Venè, R.; Bisacchi, D.; Garbisa, S.; Albini, A. Anti-invasive effects of green tea polyphenol epigallocatechin-3-gallate (EGCG), a natural inhibitor of metallo and serine proteases. *Biol. Chem.* **2002**, *383*, 101−105.
(48) Firestein, G. S. Mechanisms of tissue destruction and cellular activation in rheumatoid arthritis. *Curr. Opin. Rheumatol.* **1992**, *4*, 348−354.
(49) Pillinger, M. H.; Rosenthal, P. B.; Tolani, S. N.; Apsel, B.; Dinsell, V.; Greenberg, J.; Chan, E. S.; Gomez, P. F.; Abramson, S. B. Cyclooxygenase-2-derived E prostaglandins down-regulate matrix metalloproteinase-1 expression in fibroblast-like synoviocytes via inhibition of extracellular signal-regulated kinase activation. *J. Immunol*. **2003**, *171*, 6080−6089.
(50) Attiga, F. A.; Fernandez, P. M.; Weeraratna, A. T.; Manyak, M. J.; Patierno, S. R. Inhibitors of Prostaglandin Synthesis Inhibit Human Prostate Tumor Cell Invasiveness and Reduce the Release of Matrix Metalloproteinases. *Cancer Res.* **2000**, *60*, 4629−4637.
(51) Pachiappan, A.; Thwin, M. M.; Manikandan, J.; Gopalakrishnakone, P. Glial inflammation and neurodegeneration induced by candoxin, a novel neurotoxin from Bungarus candidus venom: global gene expression analysis using microarray. *Toxicon* **2005**, *46*, 883−899.
(52) Livak, K. J.; Schmittge, T. D. Analysis of relative gene expression data using real-time quantitative PCR and the 2(-Delta Delta C(T)) method. *Methods* **2001**, *25*, 402−408.
(53) Bax, A.; Davis, D. G. MLEV-17-based two-dimensional homonuclear magnetization transfer spectroscopy. *J. Magn. Reson.* **1985**, *65*, 355−360.

(54) Rance, M.; Sorensen, O. W.; Bodenhausen, G.; Wagner, G.; Ernst, R. R.; Wüthrich, K. Improved spectral resolution in COSY ^{1}H NMR spectra of protein via double quantum filtering. *Biochem. Biophys. Res. Commun*. **1983**, *117*, 479−485.

(55) Bax, A.; Davis D. G. Practical aspects of two-dimensional transverse NOE spectroscopy. *J. Magn. Reson*. **1985**, *63*, 207−213.

(56) Kumar, A.; Wagner, G.; Ernst, R. R.; Wuthrich, K. Buildup rates of the nuclear overhauser effect measured by two-dimensional proton magnetic resonance spectroscopy: implications for studies of protein conformation. *J. Am. Chem. Soc*. **1981**, *103*, 3654−3658.

(57) Sklenar, V. Suppression of Radiation Damping in Multidimensional NMR Experiments Using Magnetic Field Gradients. *J. Magn. Reson*. *A* **1995**, *114*, 132−135.

(58) Marion, D.; Wüthrich, K. Application of phase sensitive two-dimensional correlated spectroscopy (COSY) for measurements of ^{1}H-^{1}H spin-spin coupling constants in proteins. *Biochem. Biophys. Res. Commun.* **1983**, *113*, 967−974.

(59) Goddard, T. D.; Kneller, D. G. SPARKY3, University of California, San Francisco.

(60) Guntert, P.; Mumenthaler, C.; Wuthrich, K. Torsion angle dynamics for NMR structure calculation with the new program DYANA. *J. Mol. Biol*. **1997**, *273*, 283−298.

(61) Herrmann, T.; Guntert, P.; Wuthrich, K. Protein NMR structure determination with automated NOE assignment using the new software CANDID and the torsion angle dynamics algorithm DYANA. *J. Mol. Biol*. **2003**, *319*, 209−227.

(62) Sutcliffe, M. J. Structure determination from NMR data II. Computational Approaches. In *NMR of Macromolecules: A Practical Approach*; Roberts, G. C. K, Ed.; Oxford University Press: New York, 1993; pp 359−390.

(63) Morris, G. M.; Goodsell, D. S.; Halliday, R. S.; Huey, R.; Hart, W. E.; Belew, R. K.; Olson, A. J. Automated docking using a Lamarckian genetic algorithm and empirical binding free energy function. *J. Comput. Chem.* **1998**, *19*, 1639−1662.

JM070385X